Dynamic Theory of Type 3 Liquid Junction Potentials: Formation of Multilayer Liquid Junctions

Kristopher R. Ward, Edmund J. F. Dickinson, and Richard G. Compton*

Department of Chemistry, Physical and Theoretical Chemistry Laboratory, Oxford University, South Parks Road, Oxford, United Kingdom OX1 3QZ

Received: December 18, 2009; Revised Manuscript Received: February 22, 2010

A Nernst−Planck−Poisson finite difference simulation is used to model the dynamic evolution of a series of liquid junctions of the type $A^+X^-|B^+Y^-$, in which all ionic species are monovalent and present in equal concentration (a subset of Lingane's type 3), from a nonequilibrium initial condition to a condition of steady-state potential difference. Simulations are performed in a linear space without constrained diffusion. Analysis of the dynamics shows very good agreement with recently presented revisions for the type 1 and 2 cases [*J. Phys. Chem. B* **2010**, *114*, 187−197] Considerable deviation of the value of the limiting liquid junction potential from that predicted by the classical Henderson equation [*Z. Phys. Chem.* **1907**, *59*, 118−127] is shown in many cases and investigated as a function of the size of the various diffusion coefficients. Significantly, the formation of a "multilayer liquid junction", characterized by the existence of more than one instantaneous point of electroneutrality and thus more than one stationary point in the electric field (in a finite range of space), is inferred for the first time in a number of cases. The conditions for such a multilayer liquid junction are determined.

1. Introduction

1.1. Traditional Concepts and Recent Innovations. The formation of a liquid junction occurs upon contact between two electrolyte solutions as a result of the charge separation arising when ionic species have unequal diffusion coefficients. Lingane[1] classified liquid junctions into 3 types. Type 1 is a junction of two solutions of common phase but different concentrations, whereas type 2 is a junction of two solutions of different phase but common concentration. The type 3 classification encompasses all other types of liquid junctions.

The electric field resulting from unequal rates of diffusion accelerates the transport of the initially slower species and retards that of the initially more rapid species. Under the classical liquid junction model of Nernst and Planck,[2−4] the electric field will develop in time until the discrepancy in the diffusive flux of one or more species arising from unequal diffusion coefficients is precisely balanced by their opposite migrational attraction. At this point, it was previously assumed that the system had attained equilibrium and therefore the potential difference and the electric field both maintained a steady state. This steady-state condition was derived by arbitrarily confining the junction to a boundary layer of finite length.[4] Perram et al.[5] attacked the unphysical nature of finitely positioned Dirichlet boundary conditions and discussed the revision of the general case when the junction is constrained. Dickinson et al.[6] recently demonstrated that for unconstrained type 1 and 2 junctions, true equilibrium cannot be attained in finite time. Instead, the spatial extent of the junction, being the range over which the electric field is nonzero, continues to grow with increasing time. The electric field simultaneously relaxes back to zero at infinite time, such that the potential difference over all space remains constant. The liquid junction may therefore be thought of as a type of parallel plate capacitor, the plates representing the volume of solution on each side of the position of maximum electric field with a short time "charging" in which the liquid junction potential increases, followed by a long time "discharging" where the potential is constant as the junction is expanding.

This study intends to extend this theory from type 1 and type 2 to the general type 3 case. Investigation will be limited to a common subset of type 3 junctions, those of the form $A^+X^-|B^+Y^-$ in which all ionic species are monovalent and present in equal concentration.

Nernst−Planck−Poisson finite difference simulation is employed together with some mathematical analysis at low time to determine the dynamical behavior of such a system. The alteration to the classical model of liquid junction potentials proposed[6] for types 1 and 2 is confirmed to be equally valid for the AX|BY case, and the implicit inaccuracy of the classical Henderson equation (below) is discussed. Additionally, we present, for a number of cases, the new physical insight of a multilayer liquid junction in which, as demonstrated in Figure 1, the electric field has multiple maxima within the junction range. Figure 2 shows the change in potential over the same spatial range. We use the term multilayer because the occurrence of multiple maxima indicates that the distribution of charge alternates through the junction; there are effectively multiple capacitive "plates" of solution which are dynamically charging and discharging in series. Therefore, locally to the junction center, the perceived electric field may be opposite to that which would be indicated by the overall potential difference across the solution. The authors are not aware of existing experimental evidence for such effects in the literature, though it is expected that this paper will encourage experimental work in this area that will both confirm the predictions given and identify the conditions under which the effects are maximal.

1.2. Henderson Equation. The Henderson equation,[7,8] although inexact for all but the type 1 case[9] (as discussed in

* To whom correspondence should be addressed. Fax: +44 (0) 1865 275410. Tel: +44 (0) 1865 275413. E-mail: richard.compton@chem.ox.ac.uk.

10.1021/jp911986k
Published on Web 03/15/2010

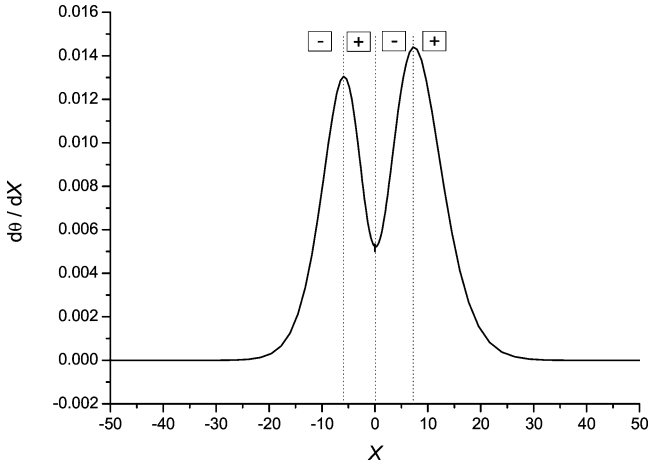

Figure 1. A typical electric field profile for a type 3 system displaying a multilayer liquid junction at some time after the system has reached a steadystate liquid junction potential. Dotted lines indicate planes of electroneutrality. $D'_A = 2$, $D'_X = 1$, $D'_B = 0.875$, $D'_Y = 0.5$.

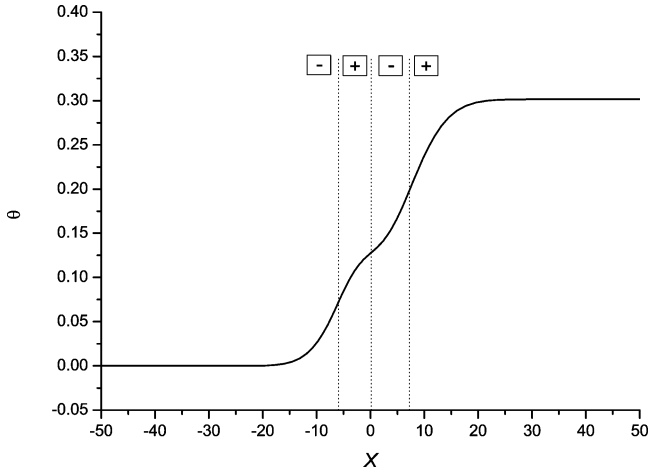

Figure 2. The potential profile of the system pictured in Figure 1. Dotted lines indicate planes of electroneutrality.

section 3.2), is nevertheless a useful tool in predicting the approximate magnitude of the limiting liquid junction potential, $\Delta\theta_{LJP,SS}$, given the charges, z_q, diffusion coefficients, D_q, and initial bulk concentrations, C_q, of all species q in the left (L) and right (R) phases of the junction

$$\Delta\phi_{LJP,SS} = \frac{\sum_q \frac{|z_q|D_q}{z_q}(C_{q,R} - C_{k,L})}{\sum_q |z_q|D_q(C_{q,R} - C_{q,L})}\frac{RT}{F}\ln\left(\frac{\sum_q |z_q|D_q C_{q,L}}{\sum_q |z_q|D_q C_{q,R}}\right) \quad (1.1)$$

where R, T, and F have their usual meanings and activity and concentration are assumed to be equivalent.

2. Theoretical Model

2.1. Liquid Junction Model. Two solutions of binary monovalent electrolytes, potentially of different concentrations, are separated by a hypothetical infinitesimal barrier which is suddenly removed, allowing the solutions to diffuse into one another. As the solutions are homogeneous within all planes parallel to the junction, mass transport may be neglected in all axes except for that perpendicular to the junction (defined as x). The flux of each species q at any point in the solution is described by the Nernst−Planck equation

$$J_q = -D_q\left(\frac{\partial C_q}{\partial x} + \frac{z_q F}{RT}C_q\frac{\partial\phi}{\partial x}\right) \quad (2.1)$$

where J_q is the x component of the flux vector for species q and ϕ is the potential. The first term is the diffusional contribution, and the second is the migrational one. By conservation of mass, the space−time evolution of C_q is given by

$$\frac{\partial C_q}{\partial t} = -\frac{\partial J_q}{\partial x} \quad (2.2)$$

Consequently

$$\frac{\partial C_q}{\partial t} = D_q\left(\frac{\partial^2 C_q}{\partial x^2} + \frac{z_q F}{RT}\frac{\partial}{\partial x}\left(C_q\frac{\partial\phi}{\partial x}\right)\right) \quad (2.3)$$

The potential at any point must further satisfy the Poisson equation

$$\frac{\partial^2\phi}{\partial x^2} = \frac{-\rho}{\epsilon_s\epsilon_0} \quad (2.4)$$

where ϵ_s is the solvent dielectric constant, ϵ_0 is the permittivity of free space, and ρ is the local charge density

$$\rho = F\sum_q z_q C_q \quad (2.5)$$

Thus, we obtain the Nernst−Planck−Poisson (NPP) equation set

$$\left(\frac{\partial^2 C_q}{\partial x^2} + \frac{z_q F}{RT}\frac{\partial}{\partial x}\left(C_q\frac{\partial\phi}{\partial x}\right)\right) - \frac{1}{D_q}\frac{\partial C_q}{\partial t} = 0 \quad (2.6)$$

for each species, k and

$$\frac{\partial^2\phi}{\partial x^2} + \frac{F}{\epsilon_s\epsilon_0}\sum_q z_q C_q = 0 \quad (2.7)$$

2.2. Normalization. By use of the following normalization conditions, we can render the NPP set dimensionless

$$c_q = \frac{C_q}{C^*_{Q,R}} \qquad \theta = \frac{F}{RT}\phi \qquad D'_q = \frac{D_q}{D_Q}$$

where concentration and diffusion coefficients are normalized against the bulk concentration of a standard species (Q) on the right-hand side of the junction. By defining the dimensionless time and space coordinates as

$$X = kx \qquad \tau = k^2 D_Q t \qquad \text{where } k^2 = \frac{F^2 C^*_Q}{RT\epsilon_s\epsilon_0}$$

we obtain the dimensionless NPP equation set

$$\frac{\partial^2 c_q}{\partial X^2} + z_q\frac{\partial}{\partial X}\left(c_q\frac{\partial\theta}{\partial X}\right) - \frac{1}{D'_q}\frac{\partial c_q}{\partial\tau} = 0 \quad (2.8)$$

for all species q and

$$\frac{\partial^2\theta}{\partial X^2} + \sum_q z_q c_q = 0 \quad (2.9)$$

The physical meaning of k may be identified by considering the conventional definition of the Debye length x_D, giving the mean radius of the ionic atmosphere of a binary electrolyte as

$$x_D = \sqrt{\frac{RT\epsilon_s\epsilon_0}{2F^2C^*}} = \frac{k^{-1}}{\sqrt{2}} \quad (2.10)$$

2.3. Boundary Conditions. The NPP equations must be solved subject to suitable boundary conditions. The outer boundaries are taken at a distance where they will vastly exceed the diffusion layer throughout the simulation time. The maximum value of X used in the simulation, X_{max}, is hence defined as

$$X_{max} = 6\sqrt{D\tau_{max}} \quad (2.11)$$

where D is the greatest normalized diffusion coefficient. The thickness of the diffuse layer is $(2D\tau)^{1/2}$ from Einstein's equation; therefore, this value is chosen as being suitably far above it.

We assume the concentrations $c_q(X,\tau)$ of the ions at the boundaries are constant and equal to their bulk values (Dirichlet boundary condition), i.e. for all τ:

$$X \to +\infty \quad c_q = c^*_{q,R} \qquad X \to -\infty \quad c_q = c^*_{q,L}$$

As there is no exchange of material at the boundaries, the simulation space is a Gaussian box of zero enclosed electric charge. Therefore, the electric field is zero at the boundaries, again at all τ

$$X \to \pm\infty \quad \frac{\partial\theta}{\partial X} = 0$$

2.4. Numerical Methods. For simulation purposes, an altered form of the NPP equations is used, where the Poisson equation is substituted into the Nernst−Planck equation

$$\frac{\partial^2 c_q}{\partial X^2} - z_q c_q \sum_q z_q c_q + z_q \frac{\partial\phi}{\partial X}\frac{\partial c_q}{\partial X} - \frac{1}{D_q}\frac{\partial c_q}{\partial \tau} = 0 \quad (2.12)$$

The one-dimensional simulation space is divided into $2n + 1$ points labeled X_{-n} to X_n, with $X_0 = 0$ as the central point. The liquid junction potential, $\Delta\theta_{LJP}$, is extracted as $\theta_n - \theta_{-n}$. The simulation uses expanding space and time grids such that there is a dense region of regular space points close to the junction, expanding proportionally to X on each side beyond some characteristic point X_s (the switching point). For point X_q at positive i

$$X_i = \begin{cases} X_i = X_{i-1} + \gamma_X X_s & \text{for } X < X_s \\ X_i = X_{i-1} + \gamma_X X_{i-1} & \text{for } X \geq X_s \end{cases} \quad (2.13)$$

where γ_X is the grid expansion coefficient; for negative i, $X_{-i} = -X_i$. The time grid is defined using the same technique; γ_T and τ_s denote the time grid expansion coefficient and the time switching point, respectively.

The simulation uses a fully implicit centrally differenced finite difference discretization scheme. The set of nonlinear simultaneous equations for all chemical species and the potential at every space step may then solved using the iterative Newton−Raphson method (Supporting Information).

In a convergence study, simulation parameters that gave the most favorable compromise between accuracy and run time were found to be $\gamma_X = 10^{-3}$; $X_s = 10^{-6}$; $\gamma_\tau = 2 \times 10^{-4}$; $\tau_s = 10^{-2}$; and $\epsilon = 10^{-3}$. This led to a run time of approximately 3 h depending on the rate of convergence, while giving at least 99.9% of the accuracy of a parameter set requiring a 4-fold increase in run time.

All simulations were programmed in C++ and run on a desktop computer with two quad core Intel Xeon 2.27 GHz Processors with 2.25GB of RAM.

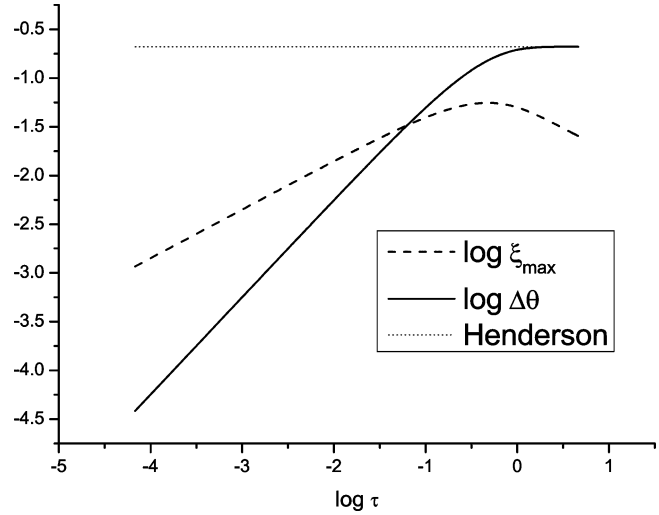

Figure 3. The evolution of the maximum electric field $(\partial\theta/\partial X|_{max})$ and liquid junction potential $(\Delta\theta_{LJP})$ for the equimolar system KNO_3|NaCl.

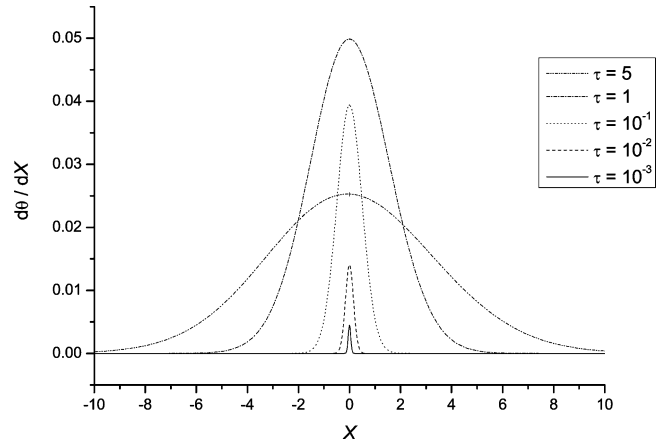

Figure 4. Electric field profiles at various times for the type 3 system KNO_3|NaCl.

3. Theoretical Results and Discussion

3.1. Exemplar Type 3 Liquid Junction: KNO_3|NaCl. The dynamics of liquid junction formation for the equimolar system KNO_3|NaCl were investigated ($D'_{K^+} = 1.467$, $D'_{Na^+} = 1$, $D'_{NO_3^-} = 1.426$, and $D'_{Cl^-} = 1.524$ at 298 K and at infinite dilution[10]). The system was chosen as a starting point for investigation as the four species are common inert ions in electrolytic solution, and the variation in diffusion coefficients in this system is modest.

The simulation was continued up until some time τ_{SS} where the potential difference remains approximately constant, that is, a limiting liquid junction potential has been reached. The condition for termination of the simulation was

$$0.998|\Delta\theta_{LJP}(\tau)| \leq |\Delta\theta_{LJP}(\tau/2)| \quad (3.1)$$

At this time, a value for the limiting liquid junction potential was recorded. In this case, very close agreement (<0.01%) with the Henderson equation was observed with a simulated value of $\Delta\theta_{LJP,SS} \approx 5.37$ mV.

3.1.1. Trends in $\Delta\theta_{LJP}$ and ξ_{max}. The potential difference across the junction, $\Delta\theta_{LJP}$, and maximum electric field, $\xi_{max} = (\partial\theta/\partial X)$, for the KNO_3|NaCl system are plotted on a logarithmic scale as a function of τ (Figures 3 and 4) to show their development. Note that the maximum electric field is not

necessarily the same as the field at $X = 0$ since the junction may be mobile.[6] These plots demonstrate that the electric field associated with unequal mass transport achieves a maximum of ~0.3 MV m^{-1} at $t \approx 7$ ns.

The dynamics of this type 3 junction show very good agreement with the type 1 and 2 cases.[6] Prior to the time of maximum field, τ_{trs}, $\Delta\theta_{LJP}$ increases proportionally to τ, and ξ_{max} increases proportionally to $\tau^{1/2}$. After τ_{trs}, $\Delta\theta_{LJP}$ approaches a limiting value ($\propto\tau^0$) whereas ξ_{max} relaxes as $\tau^{-1/2}$. This indicates that the junction charge now decreases with increasing τ. Also, after τ_{trs}, the spatial extent of the junction increases as $\tau^{1/2}$. It is also observed that the rate of discharge of the electric field is proportional to $\tau^{1/2}$, which explains why a limiting $\Delta\theta_{LJP}$ is reached even though the system is not at steady state. At long times, the position of the junction, being the point of maximum electric field and the point of electroneutrality, moves away from $X = 0$ (the initial position of the junction) due to competition between unequal mass transport and the developing electric field. It should be noted, however, that the deviation is small in the case of types 2 and 3, whereas a significant displacement from $X = 0$ was observed for the type 1 case. Furthermore, the concentration profiles of the ionic species become increasingly asymmetric in this range.

3.1.2. Zero-Feedback Approximation as $\tau \rightarrow 0$. Some insight into the limiting behavior of the type 3 (AX|BY) liquid junction as $\tau \rightarrow 0$ may be gained by means of a zero-feedback approximation. At short time, the magnitude of the electric field is vanishingly small, such that the motion of charged species in the system may be considered to be solely due to diffusion and the effects of migration can be ignored. Ignoring migration, the solutions to the diffusion equation may be substituted into the Poisson equation, which may then be integrated to find an approximate electric field (mathematical details may be found in the Appendix)

$$\left.\frac{\partial\theta}{\partial X}\right|_{max} = -2\sqrt{\frac{\tau}{\pi}}\cdot\sum_q z_q\beta_q\sqrt{D'_q} \quad \text{for all species } q \qquad (3.2)$$

where

$$\beta_q = \frac{c_{q,R} - c_{q,L}}{2} \qquad (3.3)$$

The electric field itself may then be integrated, yielding an equation for the liquid junction potential as $\tau \rightarrow 0$

$$\Delta\theta_{LJP} = -2\tau\sum_q z_q\beta_q D'_q \qquad (3.4)$$

Figure 5 shows the strong agreement between these results and the short time values of $\Delta\theta_{LJP}$ and $-\xi_{max}$.

3.2. Type 3 Henderson Deviations. Asymptotic analysis performed by Hickman[9] has shown that for the type 2 and 3 cases, the Henderson equation is not exact and in fact may be derived as the first term in an expansion for the $\tau \rightarrow \infty$ solutions in a small parameter

$$\mu = \frac{D'_{max} - D'_{min}}{D'_{max} + D'_{min}} \qquad (3.5)$$

It is therefore not unreasonable to conclude that for the type 3 case, the deviations observed will be significant, where D'_{max} and D'_{min} differ substantially and hence higher powers of μ are significant.

A series of equimolar type 3 liquid junctions were simulated with varying diffusion coefficients. The ratio D'_{L-}/D'_{R-} was kept constant at 2 while the ratios D'_{L+}/D'_{L-} and D'_{R+}/D'_{R-} were varied

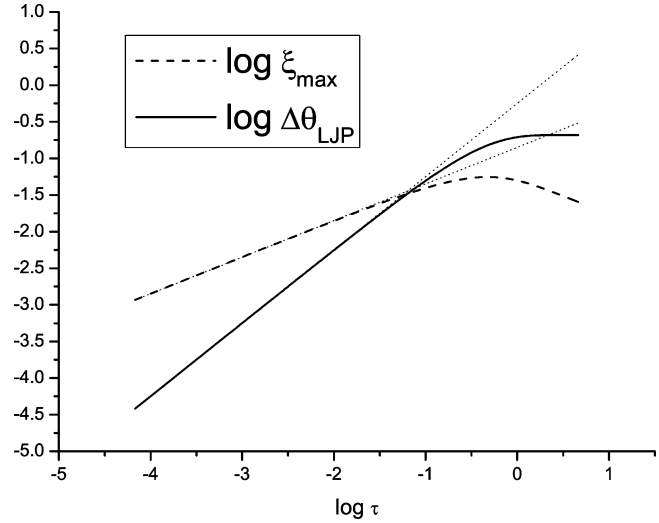

Figure 5. Limiting behavior as $\tau \rightarrow 0$ of the maximum electric field (ξ_{max}) and liquid junction potential ($\Delta\theta_{LJP}$) for the type 3 equimolar system KNO_3|NaCl.

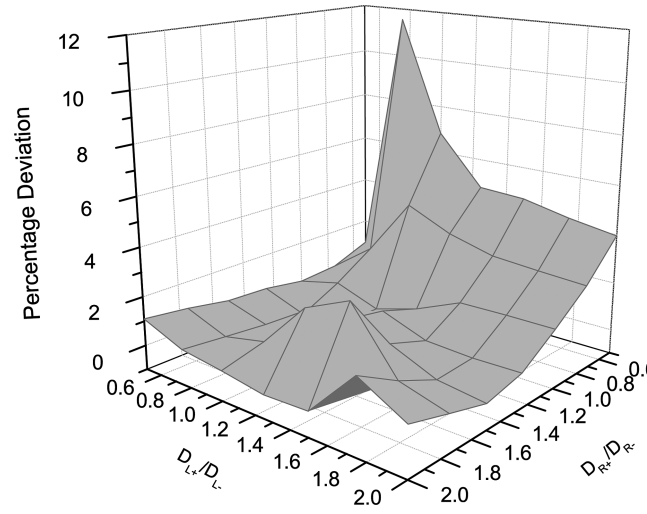

Figure 6. Percentage deviation of $\Delta\theta_{LJP}$ from the value predicted by the Henderson equation for a range of type 3 systems AX|BY where $D'_{L-}/D'_{R-} = 2$.

over the set of values 2, 1.75, 1.5, 1, 0.66, 0.57, and 0.5, giving 49 simulated cases in total. Figure 6 shows the percentage difference between the value of $\Delta\theta_{LJP,SS}$ from the simulation and that predicted by Henderson for these cases. Note that the condition for the steady state was the same as that used above.

One anomaly of particular interest is the case where $\{D'_{L+} = 1.5, D'_{L-} = 1, D'_{R+} = 1, D'_{R-} = 0.5\}$, for which the Henderson equation predicts a value for $\Delta\theta_{LJP}$ of 0 but where the simulation gives a small, finite value of $\Delta\theta_{LJP}$ with junction dynamics correlating with those generally observed. In this case, the percentage deviation from the Henderson equation is formally infinite, and this must be entirely accounted for by second- and higher-order correction terms to the Henderson equation. Aside from this one singularity, the Henderson equation deviation ranges from very small (<0.02%) to very significant (>8%), over the relatively limited range of diffusion coefficient ratios in the simulated set of systems. It was generally observed that a greater deviation from the Henderson equation occurred when both the cation and anion on one side of the junction had greater diffusion coefficients than their counterparts on the other side, while they themselves had similar diffusion coefficients.

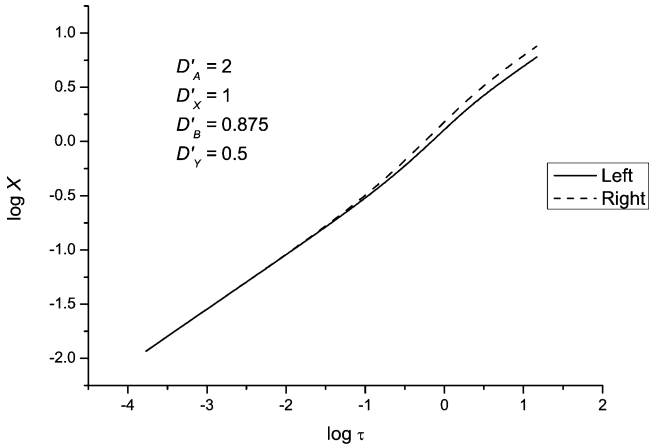

Figure 7. Displacement of electric field stationary points from $X = 0$ for a type 3 system displaying a multilayer liquid junction.

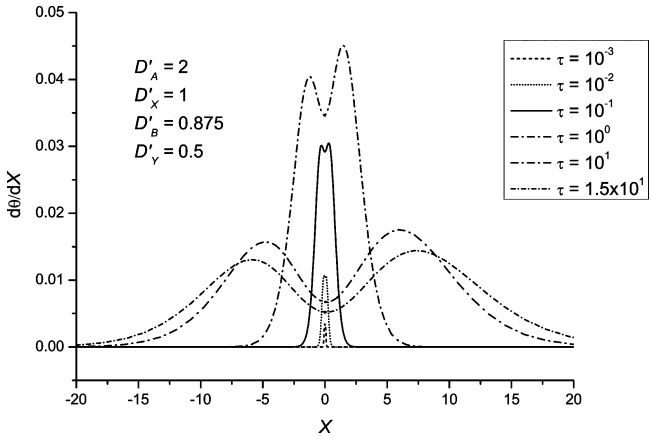

Figure 8. Electric field profiles at various times for a type 3 system displaying a multilayer liquid junction.

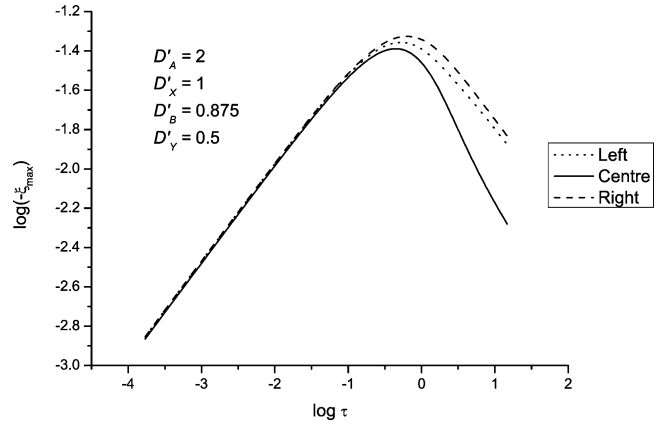

Figure 9. Evolution of electric field stationary points for a type 3 system displaying a multilayer liquid junction.

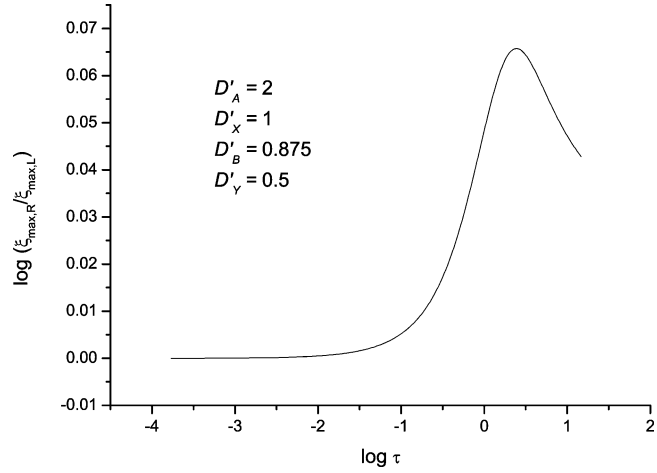

Figure 10. Evolution of junction asymmetry for a type 3 system displaying a multilayer liquid junction.

In consideration of the work of Hickman,[9] the simulated values must more closely represent reality than those predicted by the Henderson equation since there is no imposition of electroneutrality or artificial constraint of the liquid junction in these studies.

On the basis of this, a real-world system, NaOAc|KOH, was also simulated, with a high deviation expected. The observed deviation was 1.55% of the Henderson value, that is, a value of $\Delta\theta_{LJP,SS} = 20.4$ mV compared to 20.72 mV from the Henderson equation.

3.3. Formation and Dynamics of a Multilayer Liquid Junction. From the above investigations into deviations from the Henderson equation, it was observed that under certain conditions, the nature of which are discussed below, the AX|BY system had a tendency to form a multilayer liquid junction characterized by three points of electroneutrality (at finite X) and thus three corresponding stationary points in the electric field, as shown in Figure 1. In these cases, the true liquid junction position is no longer well-defined, and the system may effectively be thought of as two solution-phase "capacitors" in series that are charging/discharging into one another dynamically.

As demonstrated in Figure 1, a typical plot of $|\partial\theta/\partial X|$ for a type 3 junction ($D'_A = 2$, $D'_X = 1$, $D'_B = 0.875$, and $D'_Y = 0.5$) at finite time shows a local central minimum at or near $X = 0$ (the initial junction location) and two satellite maxima. At $\tau > 0$, the spatial location of the central minimum, which remains loosely analogous to the location of the liquid junction, moves away from $X = 0$ in the same manner as the single junction case. At the same time, the displacement from $X = 0$ of both satellite maxima increases with increasing τ (Figure 7). The magnitudes of these maxima increase (asymmetrically) up to some characteristic time, τ_{trs}, after which they relax exponentially back to zero as $\tau \rightarrow \infty$. Note that the values of τ_{trs} for each maximum do not necessarily coincide. Figure 8 shows the evolution of the electric field profile for a system with a multilayer liquid junction, Figure 9 shows the evolution of the magnitude of stationary points in the electric field, and Figure 10 shows the evolution of the asymmetry of the junction pair for the same system defined as $\xi_{max,R}/\xi_{max,L}$.

3.3.1. Agreement with Theory. From the $\tau \rightarrow 0$ analysis presented in detail in the Appendix, to the first approximation

$$\frac{\partial\theta}{\partial X} = -\sum_q z_q\beta_q\left(X\mathrm{erf}\left(\frac{X}{2\sqrt{D'_q\tau}}\right) + 2\sqrt{\frac{D'_q\tau}{\pi}}\exp(-X^2/4D'_q\tau)\right) \quad (3.6)$$

Figure 11 shows a comparison between this equation and the results of the simulation at $\tau = 0.001$ for this system with extremely strong agreement evident.

3.3.2. Conditions of Multilayer Liquid Junction Formation. In order to gain a greater understanding of the nature of multilayer liquid junction formation, it is useful to examine the conditions under which such a system arises. A junction occurs at a point of electroneutrality, that is, when there is a stationary point in the electric field or, equivalently, when the electric field gradient is 0

$$\frac{\partial^2\theta}{\partial X^2} = -\sum_q z_q c_q = 0 \tag{3.7}$$

from the Poisson equation. Now as at short time (Appendix)

$$c_q = \alpha_q + \beta_q \cdot \mathrm{erf}\left(\frac{X}{2\sqrt{D'_q\tau}}\right) \tag{3.8}$$

and since

$$\sum_q z_q \alpha_q = 0 \tag{3.9}$$

assuming the solutions are initially electroneutral, it is clear that as $\tau \to 0$, there will be a stationary point in the electric field at any point X where

$$\sum_q z_q \beta_q \mathrm{erf}\left(\frac{X}{2\sqrt{D'_q\tau}}\right) = 0 \tag{3.10}$$

Unfortunately this cannot be solved for X directly, and therefore, it cannot be used to find the position of any stationary points (aside from the trivial examples of 0 and $\pm\infty$); however, it can be used to infer the existence of nontrivial solutions and thus of a multilayer liquid junction. In all simulations, it was found that if multiple maxima occurred as $\tau \to 0$, they were maintained as $\tau \to \infty$.

For the equimolar case, the set of coefficients $z_q\beta_q$ are -0.5, $+0.5$, $+0.5$, and -0.5 for k = A, X, B, and Y, respectively. Therefore, eq 3.10 reduces to

$$\delta_X - \delta_A + \delta_B - \delta_Y = 0 \tag{3.11}$$

where

$$\delta_q = \mathrm{erf}\left(\frac{X}{2\sqrt{D'_q\tau}}\right) \tag{3.12}$$

As the error function is a monotonic odd function, it is necessarily true that if X is a root of the equation, so is $-X$. Here, we consider only positive values of X. We therefore require by continuity that if a root exists over $0 < X < \infty$, then either the root exists as a stationary point, which we exclude as a transitional case, or for some X between 0 and ∞

$$\delta_X - \delta_A + \delta_B - \delta_Y > 0 \tag{3.13}$$

and that for some other range of X within the same limits

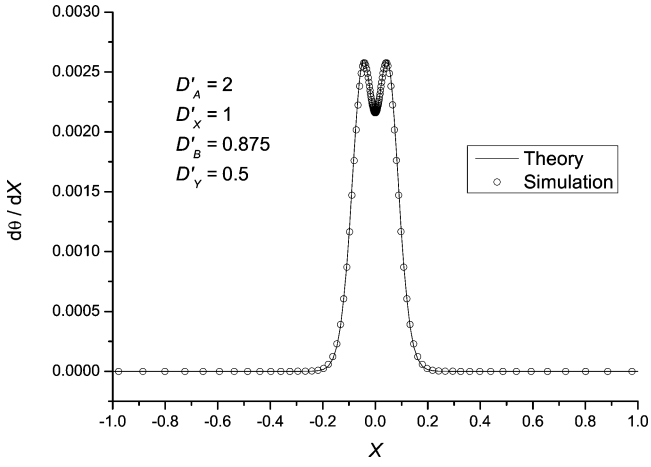

Figure 11. Electric field profile at $\tau = 0.001$ (theory and simulation) for a type 3 system displaying a multilayer liquid junction.

TABLE 1: Error Function Conditions

for some values(s) $X > 0$	for some other value(s) $X > 0$
$\delta_X - \delta_Y > \delta_A - \delta_B$ (1)	$\delta_X - \delta_Y < \delta_A - \delta_B$ (2)
$\delta_X - \delta_A > \delta_Y - \delta_B$ (3)	$\delta_X - \delta_A < \delta_Y - \delta_B$ (4)
$\delta_X + \delta_B > \delta_A + \delta_Y$ (5)	$\delta_X + \delta_B < \delta_A + \delta_Y$ (6)

$$\delta_X - \delta_A + \delta_B - \delta_Y < 0 \tag{3.14}$$

The conditions expressed in Table 1 therefore follow.

If we set the order of the junction such that the cation on the left-hand side has a lower diffusion coefficient than that on the right, so that $\delta_A > \delta_B$, it necessarily follows that $\delta_X > \delta_Y$, or else, condition (1) in Table 1 is not satisfied, and there can be no nontrivial solutions. Similarly, if $\delta_X > \delta_A$, then it follows from condition (3) that $\delta_Y > \delta_B$ or vice versa for the same reasons. If we rearrange conditions (5) and (6) such that

$$2(\delta_X - \delta_A) > (\delta_Y - \delta_A) - (\delta_X - \delta_B) \quad \text{for some range of } X > 0 \tag{3.15}$$

and

$$2(\delta_X - \delta_A) < (\delta_Y - \delta_A) - (\delta_X - \delta_B) \quad \text{for some other range of } X > 0 \tag{3.16}$$

we can see that if $\delta_X > \delta_A$, then $(\delta_Y - \delta_A) > (\delta_X - \delta_B)$ at some range of X, and therefore, if $\delta_X > \delta_B$, it follows that $\delta_Y > \delta_A$. Furthermore. we can see that if $\delta_A > \delta_X$, then $(\delta_Y - \delta_A) < (\delta_X - \delta_B)$ at some range of X; therefore, if $\delta_X < \delta_B$, it follows that $\delta_Y < \delta_A$. For a junction arranged such that $D'_{R+} > D'_{L+}$, there are 12 possible ways of ordering the diffusion coefficients. The above eliminates nine of the possibilities; therefore, in order for a multilayer liquid junction to be formed in a junction arranged such that $D'_{R+} > D'_{L+}$, it is necessary that one of the following conditions be met

$$D'_{L+} < D'_{R+} \le D'_{L-} < D'_{R-} \tag{3.17}$$

or

$$D'_{L+} < D'_{L-} \le D'_{R+} < D'_{R-} \tag{3.18}$$

or

$$D'_{L-} < D'_{R-} \le D'_{L+} < D'_{R+} \tag{3.19}$$

where L and R are the left- and right-hand sides of the junction, respectively, with the side chosen as R being that where the cation diffuses most rapidly. It is also necessary that

$$D_{R+} \neq D_{R-} \qquad \text{and that } D_{L+} \neq D_{L-} \tag{3.20}$$

Note that these conditions are necessary but not sufficient conditions for the formation of a multilayer liquid junction. Figure 12 shows the effect on the electric field of an AX|BY system that results from varying the value of D'_A from twice that of D'_X to less than the value of D'_B (at which point the multilayer junction is no longer present) and finally to the value of D'_Y, which is equivalent to a type 2 system (keeping the other diffusion coefficients fixed as $D'_X = 1$, $D'_B = 0.875$, and $D'_Y = 0.5$). As the system shifts from the type 3 to the type 2 limit, it is observed that the magnitude of the asymmetry of the satellite maxima, being defined as $\xi_{max,R}/\xi_{max,L}$, decreases. Also, the magnitude of the maximum electric field ($-\xi$) at the maxima decreases, and that at the minimum increases. It should be noted that the inflection in the electric field is not directly observable simply from the measurement of the potential difference across the whole solution.

An example of a real world system, NaOAc|$KClO_4$ ($D'_{Na} = 1.22$, $D'_{OAc} = 1$, $D'_K = 1.797$, $D'_{ClO_4} = 1.66$[10]), is shown in Figure 13. The electric field was found to achieve a maximum at $\tau =$

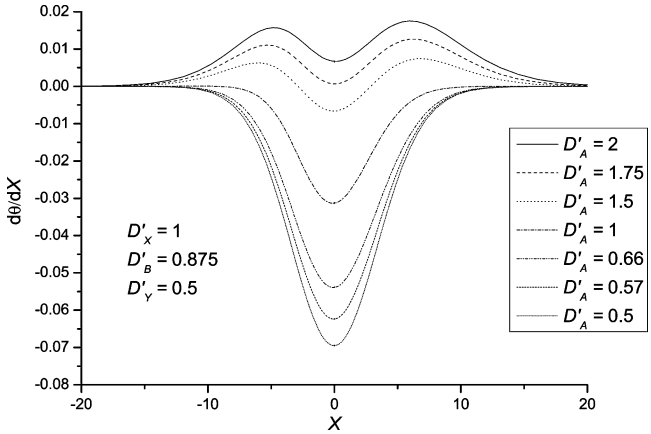

Figure 12. Electric field profiles at $\tau = 10$ for a range of type 3 systems with varying D'_A.

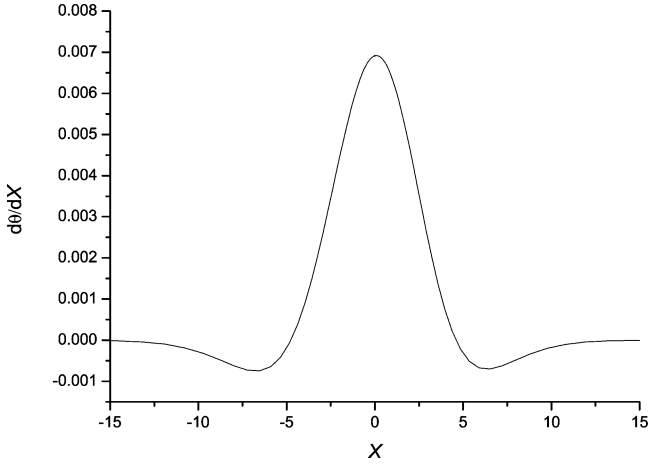

Figure 13. Electric field profile at $t = 68$ ns for the type 3 system NaOAc| $KClO_4$, displaying a multilayer liquid junction. $D'_{Na} = 1.22$, $D'_{OAc} = 1$, $D'_K = 1.797$, $D'_{ClO_4} = 1.66$.[10]

0.55. In dimensional units, the maximum field is 0.07 MV m^{-1} at 9.3 ns after contact between the solutions and a limiting liquid junction potential of 7.48 mV, which is reached after 66 ns.

4. Conclusions

An in-depth analysis of the dynamical behavior of liquid junctions of Lingane's type 3 has been performed, with agreement between type 3 dynamics and those reported for types 1 and 2 being evident. Additionally, the deviation of the value of the limiting liquid junction potential from that predicted by the Henderson equation has been shown to be quite significant under many sets of initial conditions for the type 3 case. Further, the new physical insight of a multilayer liquid junction, in which the electric field has multiple maxima within the junction range, has been presented and the conditions of its formation discussed. Although no experimental corroboration has been presented, the authors expect that this article will prompt experimental work in this area that will both validate the model and its predictions and identify the conditions under which the effects are most significant.

Acknowledgment. E.J.F.D. thanks St John's College, Oxford, for funding. E.J.F.D. additionally thanks Paul Crewe (Mathematical Institute, University of Oxford) for continued discussion on our mathematical analyses.

Appendix

Limiting $\tau \rightarrow 0$ Analysis by the Zero-Feedback Approximation. Let us suppose that we have initially q species with concentrations $c^*_{q,L}$ and $c^*_{q,R}$ left and right of a membrane. Let us further suppose initially that there is no feedback from the electric field upon itself or upon the mass transport of the species

$$\frac{\partial c_q}{\partial \tau} = D'_q \frac{\partial^2 c_q}{\partial X^2} \tag{4.1}$$

If initially

$$c_q(X, \tau = 0) = \alpha_q + \beta_q \cdot \mathrm{sgn}(X)$$

$$\text{where } \alpha_q = \frac{c_{R,q} + c_{L,q}}{2} \quad \beta_q = \frac{c_{R,q} - c_{L,q}}{2} \tag{4.2}$$

and for $\tau > 0$

$$c_q(X \rightarrow \pm\infty, \tau) = \alpha_q \pm \beta_q \tag{4.3}$$

then

$$c_q = \alpha_q + \beta_q \cdot \mathrm{erf}\left(\frac{X}{2\sqrt{D'_q \tau}}\right) \tag{4.4}$$

Assuming initial electroneutrality

$$\sum_q z_q c^*_{q,L} = \sum_q z_q c^*_{q,R} = 0 \tag{4.5}$$

therefore

$$\sum_q z_q \alpha_q = \sum_q z_q c^*_{L,q} + \sum_q z_q c^*_{R,q} = 0 \tag{4.6}$$

Now

$$\frac{\partial^2 \theta}{\partial X^2} + \sum_q z_q c_q = 0 \tag{4.7}$$

and hence

$$\frac{\partial \theta}{\partial X} = -\int_{-\infty}^{X} \left(\sum_q z_q \beta_q \cdot \mathrm{erf}\left(\frac{X'}{2\sqrt{D'_q \tau}}\right)\right) \mathrm{d}X' \tag{4.8}$$

$$= -\sum_q z_q \beta_q \left[X' \,\mathrm{erf}\left(\frac{X'}{2\sqrt{D'_q \tau}}\right) + 2\sqrt{\frac{D'_q \tau}{\pi}} \exp(-X^2/4D'_q \tau) \right]_{-\infty}^{X} \tag{4.9}$$

Furthermore

$$\sum_q z_q \beta_q \,\mathrm{erf}(-\infty) = -\sum_q z_q \beta_q = \frac{1}{2}\sum_q z_q c^*_{L,q} - \frac{1}{2}\sum_q z_q c^*_{R,q} = 0 \tag{4.10}$$

and as

$$\mathrm{erf}\left(\frac{X}{2\sqrt{D'_q \tau}}\right) \rightarrow 1 \quad \text{a constant, faster than } X \rightarrow \infty \tag{4.11}$$

since

$$\frac{\mathrm{d}}{\mathrm{d}X}\left(\mathrm{erf}\left(\frac{X}{2\sqrt{D'_q\tau}}\right)\right) = \frac{1}{2\sqrt{D'_q\tau}}\frac{2}{\sqrt{\pi}}\exp(-X^2/2\sqrt{D'_q\tau}) \rightarrow 0 \quad \text{faster than } X \rightarrow \infty \tag{4.12}$$

it follows that

$$\lim_{X\rightarrow-\infty}\sum_q z_q\beta_q X\,\mathrm{erf}\left(\frac{X}{2\sqrt{D'_q\tau}}\right) = -X\sum_q z_q\beta_q = 0 \tag{4.13}$$

therefore

$$\frac{\partial\theta}{\partial X} = -\sum_q z_q\beta_q\left(X\,\mathrm{erf}\left(\frac{X}{2\sqrt{D'_q\tau}}\right) + 2\sqrt{\frac{D'_q\tau}{\pi}}\exp(-X^2/4D'_q\tau)\right) \tag{4.14}$$

and since $\partial^2\theta/\partial X^2 = 0$ when $X = 0$

$$\left.\frac{\partial\theta}{\partial X}\right|_{\max} = -\sum_q z_q\beta_q\cdot 2\sqrt{\frac{D'_q\tau}{\pi}} \tag{4.15}$$

$$= -2\sqrt{\frac{\tau}{\pi}}\cdot\sum_q z_q\beta_q\cdot\sqrt{D'_q} \tag{4.16}$$

The short time limit for $\Delta\theta_{\mathrm{LJP}}$ is then found by integration

$$\Delta\theta_{\mathrm{LJP}} = \int_{-\infty}^{\infty}\frac{\partial\theta}{\partial X}\cdot\mathrm{d}X \tag{4.17}$$

$$= \int_{-\infty}^{\infty} -\sum_q z_q\beta_q\left(X\cdot\mathrm{erf}\left(\frac{X}{2\sqrt{D'_q\tau}}\right) + 2\sqrt{\frac{D'_q\tau}{\pi}}\exp(-X^2/4D'_q\tau)\right)\mathrm{d}X \tag{4.18}$$

$$= -2\tau\sum_q z_q\beta_q D'_q \tag{4.19}$$

Supporting Information Available: Details of the mathematics of the iterative Newton−Raphson method used to numerically solve the nonlinear equaton in this paper. This material is available free of charge via the Internet at http://pubs.acs.org.

References and Notes

(1) Lingane, J. J. *Electroanalytical Chemistry*, 2nd ed.; Wiley: New York, 1958.
(2) Nernst, W. H. *Z. Physik. Chem.* **1889**, *4*, 165.
(3) Planck, M. *Wied. Ann.* **1890**, *39*, 161–186.
(4) Planck, M. *Wied. Ann.* **1890**, *40*, 561–576.
(5) Perram, J. W.; Stiles, P. J. *Phys. Chem. Chem. Phys.* **2006**, *8*, 4200–4213.
(6) Dickinson, E. J. F.; Freitag, L.; Compton, R. G. *J. Phys. Chem. B* **2010**, *114*, 187–197.
(7) Henderson, P. *Z. Physik. Chem.* **1907**, *59*, 118–127.
(8) Henderson, P. *Z. Physik. Chem.* **1908**, *63*, 325–345.
(9) Hickman, H. J. *Chem. Eng. Sci.* **1970**, *25*, 381–398.
(10) Bard, A. J.; Faulkner, L. R. *Electrochemical Methods: Fundamentals and Applications*, 2nd ed.; John Wiley & Sons: New York, 2001.

JP911986K